Ding *et al. Chin. J. Mech. Eng.* (2019) 32:20
https://doi.org/10.1186/s10033-019-0331-0

Chinese Journal of Mechanical Engineering

ORIGINAL ARTICLE

Open Access

Hierarchical Optimization of Landing Performance for Lander with Adaptive Landing Gear

Zongmao Ding[1,2*], Hongyu Wu[1,3], Chunjie Wang[1,4] and Jianzhong Ding[1]

Abstract

A parameterized dynamics analysis model of legged lander with adaptive landing gear was established. Based on the analysis model, the landing performances under various landing conditions were analyzed by the optimized Latin hypercube experimental design method. In order to improve the landing performances, a hierarchical optimization method was proposed considering the uncertainty of landing conditions. The optimization problem was divided into a higher level (hereafter the "leader") and several lower levels (hereafter the "follower"). The followers took conditioning factors as design variables to find out the worst landing conditions, while the leader took buffer parameters as design variables to better the landing performance under worst conditions. First of all, sensitivity analysis of landing conditioning factors was carried out according to the results of experimental design. After the sensitive factors were screened out, the response surface models were established to reflect the complicated relationships between sensitive conditioning factors, buffer parameters and landing performance indexes. Finally, the response surface model was used for hierarchical optimization iteration to improve the computational efficiency. After selecting the optimum buffer parameters from the solution set, the dynamic model with the optimum parameters was simulated again under the same landing conditions as the simulation before. After optimization, nozzle performance against damage is improved by 5.24%, the acceleration overload is reduced by 5.74%, and the primary strut improves its performance by 21.10%.

Keywords: Landing gear, Soft landing, Sensitivity analysis, Response surfaces, Hierarchical optimization

1 Introduction

Legged lander has been used for deep space exploration because of its high landing stability and terrain adaptability [1]. In order to isolate vibration and reduce load during soft landing, the legged lander generally uses the plastic material such as honeycomb as the main absorber to design the landing gear. However, the performances of these landing gears are unable to be adjusted during soft landing. In order to cope with complex landing terrain, larger design margin should be reserved, resulting in the heavier soft landing system [2]. With the continuous progress of deep space exploration, the terrain environment of interesting regions will be more complex and harsh, and landing in multiple regions to accomplish different detection missions may be needed. So it is required that the lander has better terrain adaptability and its landing gears are reusable.

Considering those requirements, Adaptive landing gear was proposed as a possible solution. Refs. [3–5] introduced hydraulic system, intelligent materials and pyrotechnics devices into the design of landing gear to realize adaptive control. Among them, magnetorheological damper (MR damper) is widely studied because of its cheerful prospect. In Refs. [2, 6–9], the single MR damper was designed and analyzed in detail, and the equivalent mathematical model of its characteristics was obtained. Refs. [10–13], which proposed a variety of control strategies for the lander with adaptive landing gears, proved the effectiveness of adaptive gears in enhancing

*Correspondence: buaa_dzm@163.com
[1] School of Mechanical Engineering and Automation, Beijing University of Aeronautics and Astronautics, Beijing 100083, China
Full list of author information is available at the end of the article

soft landing performances. Previous studies mostly discussed the implementation of adaptive lander, and few concerned the soft landing performance optimization for the adaptive lander. But performance optimization is of great importance for the weight reduction of lander and it benefits the improvement of terrain adaptability. Existing researches about landers optimization mostly focus on conventional passive control lander [14–16]. Furthermore, the worst condition uncertainty caused by the change of design variables was ignored in the existing researches. And the selection or optimization of the parameters was just based on the typical condition, which leads to the instability of soft landing safety.

Aiming at the uncertainty of the worst condition, a hierarchical optimization method was proposed to update the worst condition dynamically during the progress optimizing the adaptive buffer parameters. First, a dynamic analysis model of adaptive lander was established, and its soft landing performance was analyzed and evaluated. Then the response surface was adopted to participate the iterative computation of hierarchical optimization. The lander with the optimized adaptive buffer was simulated. The results show that the optimization effectively improves the soft landing performance, which verifies the feasibility of the hierarchical optimization method.

2 Dynamic Model of the Lander

2.1 Configuration and Coordinate System Definition of Lander

Figure 1 shows the overall configuration of the lander studied in this paper, which consists of a main body and four symmetrically distributed landing gears (Figure 2). The main body is a mounting platform for various detecting instruments and control subsystem. All of the landing gears, with the same configuration and size, are composed of one primary strut, two secondary struts and one footpad. The connection between struts is realized through a universal joint, so as between struts and main body, while the footpad is connected with the primary strut by the ball joint. The primary struts are adaptive buffers, and the secondary ones use aluminum

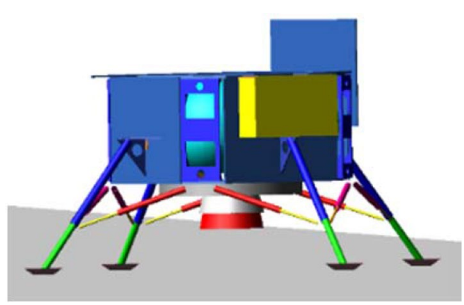

Figure 1 Configuration of the lander

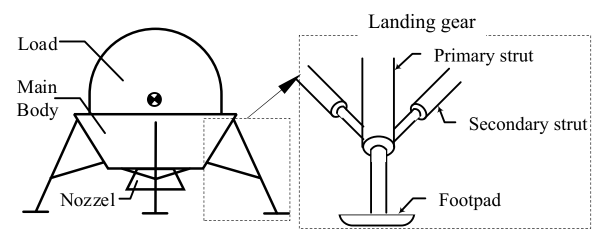

Figure 2 Main structures of the lander

honeycomb core as buffer component. The relationship of secondary strut between the cushioning force f_a and the buffering stroke d_a is shown in Figure 3, while the characteristic of primary strut will be discussed later. Take Refs. [17, 18] as reference, the structure parameters of the lander at touchdown is selected (Table 1).

The dynamic analysis model of soft landing was established by ADAMS, and gravity environment was set in the moon. The lander footpad numbering and the coordinates definition is shown in Figure 4, where O_s-$X_sY_sZ_s$ is global coordinate system, O_c-$X_cY_cZ_c$ is centroid control coordinate system, α_e is the equivalent slope of landing surface, the speed along X_s is vertical velocity v_x and the speed along X_s is horizontal velocity v_z. The rotation angles from O_s-$X_sY_sZ_s$ to O_c-$X_cY_cZ_c$ in order of Z-X-Y are defined as: ϕ (rotation about the X_s), θ (rotation about the Y_s) and ψ (rotation about Z_s). The contact force between footpad and landing surface was simulated by nonlinear spring damping model and Coulomb friction model [15].

2.2 Adaptive Buffer and Its Control Strategy

Unlike the conventional landing gears, such as honeycomb core and air bag, buffer characteristics of adaptive buffer are able to be controlled by adopting some structures or intelligent material. So the adaptability of lander equipped with this kind of buffer can be improved. Even if the adaptive control system fails, the adaptive landing gear will degenerate to the conventional passive landing gear but not palsy, which ensures the safety and reliability of the landing system [11].

Considering the maturity of techniques, MR damper was chosen as carrier for adaptive control strategy. The main components of adaptive buffer are spring and MR damper, in which the spring provides restoring force, and MR damper provides damping force. The structure of adaptive buffer is shown in Figure 5. The magnetic field strength of the coil is changed by controlling the energizing voltage, so as to dynamically adjust the damping coefficient of MR damper.

According to the existing research results, the MR damper produces a large damping force at a relatively

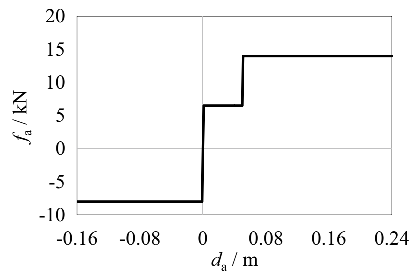

Figure 3 Force–stroke relationship of secondary strut

Table 1 Parameters of the lander at touchdown

Parameter	Value
Mass of load (kg)	1650
Mass of landing gear (kg)	15
Height of mass center (mm)	2500
Radius of footpad's lower surface (mm)	100
Distance between two adjacent footpads (mm)	4000

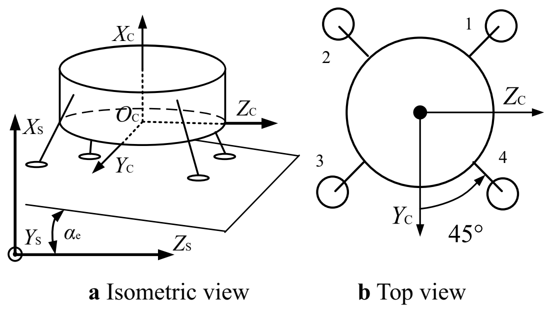

Figure 4 Definition of coordinate systems

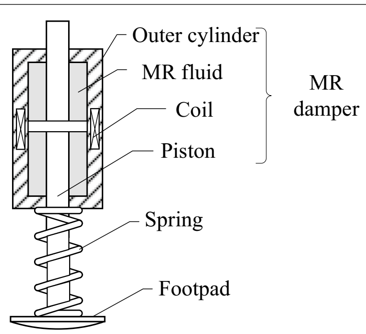

Figure 5 Sketch of adaptive buffer

small velocity (about 0.1 m/s) [19, 20]. Considering that the touchdown velocity is above 3 m/s, the lander will slow down with a large acceleration overload, which will affect the stable operation of the instruments on board and is undesired. To preserve the transportability of the strategy, the conventional linear damping force model is adopted. The damping force of MR damper is controlled to keep a linear relation with the buffer velocity by adjusting the applied current. The equivalent force of adaptive buffer can be simplified as shown in Eq. (1) [21–23]:

$$f = -c\dot{s} + ks, \tag{1}$$

where f is the equivalent force, c is the equivalent damping coefficient, k is the equivalent stiffness coefficient and s is the cushioning stroke of the buffer.

To ensure the controlling flexibility and promptness, a jump control strategy based on the minimum energy principle was adopted to realize the adaptive adjustment of the damping coefficient [13]. Considering the symmetry of the land model, the damping coefficient control function is shown as Eq. (2):

$$c_i = \frac{c_{\max} - c_{\min}}{2}\operatorname{sgn}\left[\left(-\dot{\theta} + \dot{\psi}\right)s_i\right] + \frac{c_{\max} + c_{\min}}{2}, \tag{2}$$

where c_i is the equivalent damping coefficient of damper i, and $c_{\min}$, $c_{\max}$ are the lower and upper limit to be controlled.

In the whole simulation analysis of the soft landing, the angular velocity $\dot{\theta}$, $\dot{\psi}$ of the lander and the buffer speed of the main strut $\dot{s}$ were monitored in real time through measurements. According to the Eq. (1), four cushioning forces are applied to primary struts, where the damping coefficient model is shown as Eq. (2). Finally, the independent feedback adjustment of the damping coefficients is realized.

In order to determine the initial buffer characteristic parameters of the buffer, the soft landing process is simplified as spring damping model. Under the ideal condition that four pads simultaneously touch the ground, it was required that there was no vibration during soft landing [24]. The damping ratio under above condition is chosen as 2.0 and the buffer is designed with a dynamic range ratio of 10 [25]. When the lander hits ground at the vertical speed of 3.5 m/s, the nominal buffer stroke is 0.075 m. Based on the above chosen parameters, the nominal stiffness coefficient and the maximum damping coefficient are determined according to the method described in Ref. [13]. The initial buffer characteristic parameters are listed in Table 2.

3 Simulation and Analysis for Adaptive Lander

3.1 Indicators for Soft Landing

Considering the implementation requirements of landing exploration missions, the main concerns about soft landing performance are as follows.

Table 2 Initial buffer characteristic parameters

Parameter	Value	Range
Stiffness coefficient k (N/m)	4.9×10^4	$[3 \times 10^4, 7 \times 10^4]$
Maximum damping coefficient c_{max}/(Ns/m)	5.4×10^4	$[3 \times 10^4, 7 \times 10^4]$
Dynamic range ratio $r = c_{min}/c_{max}$	0.1	[0.1, 1.0]

1) Nozzle performance against damage. Landing on regions with rough terrain may damage the nozzle due to rugged landing surface, which affects the performance of the main engine. The minimum distance between the bottom of the nozzle and the landing surface is chosen as the evaluation index. The larger the index is, the better.
2) Acceleration overload. Considering the acceleration tolerance of astronauts and the instruments equipped on the lander, the overload during the soft landing should not exceed 15g to ensure the progress of the detection mission. The maximum acceleration during soft landing is selected as an index to access the overload characteristic. The smaller the value is, the better.
3) Buffer performance. Considering the uncertainty of the environment of the target landing regions, the buffer performance should meet the demand of the worst condition. The maximum buffer stroke during soft landing is selected as one of the indexes. And a smaller value means that the volume and weight of the landing gear can be reduced correspondingly, which is beneficial to soft landing.
4) Landing stability. A vertical plane passing through the center of two adjacent footpads, which is parallel to the gravity vector, is defined as an "stability wall" [26]. Since the lander has four legs, there are four such walls. If the centroid of the lander exceeded the enclosure formed by the four stability walls, the landing was considered to be unstable. Here stability distance T is introduced as a parameter measuring the minimum distance between the centroid of the lander and four stability walls during each soft landing. If T remained positive, the landing was declared to be stable.

However, stability is not the only requirement for a successful soft landing. Here, the other indexes except the landing stability were grouped as performance indexes to access the soft landing systematically. In summary, the four selected indicators are listed in Table 3.

3.2 Analysis of Landing Performance

Based on theory of probability and statistics, experimental design is a scientific and reasonable arrangement of experiments. It extracts a number of sample points within the design interval to better reflect the characteristics of the whole space. To analyze the soft landing performance of adaptive lander under various conditions, optimal Latin hypercube method was adopted. As a result, 36 conditions were screened out as the inputs of experimental design. Taking returned terrain data and current hovering control ability as references, the selected soft landing conditioning factors and its ranges are listed in Table 4 [15], where the horizontal velocity v_z and the control errors of rolling angle ψ and pitching angle θ are ignored.

The dynamic simulations of the 36 soft landing conditions were carried out, and corresponding soft landing performance data were obtained, which will be mentioned later. In order to display the soft landing process more intuitively, typical 2-2 condition (Table 5) was selected to be analyzed in detail [27]. Based on the simulation results of 2-2 condition, the relationships between damping coefficient of primary buffer, landing stability index and three performance indexes against time increment are shown respectively in Figures 6, 7, 8, 9 and 10.

According to the above figures, during the whole soft landing process, the damping coefficients of the four adaptive buffers are dynamically adjusted as the attitude

Table 4 Soft landing conditioning factors

Condition	Range
v_x (m/s)	[3, 4]
φ (°)	[0, 45]
μ	[0.3, 0.7]
α_e (°)	[0, 10]

Table 3 Indicators for soft landing

Indicator		Parameter	Sign
Performance indexes	Nozzle performance against damage	Minimum distance between the bottom of the nozzle and the landing surface (mm)	U
	Acceleration overload	Maximum acceleration during soft landing (g)	L
	Buffer performance	Four maximum buffer strokes during soft landing (mm)	S
Landing stability index		Minimum distance between the centroid of the lander and four stability walls (mm)	T

of the lander changes, which leads to a stable soft landing. However, buffer parameters selected above based on only an ideal working condition where four legs hit the ground at the same time. While for deep space exploration mission, there is great uncertainty about the terrain and condition of interesting regions. So it is necessary to optimize the buffer parameters based on the uncertainty of landing conditions, so as to enhance the landing adaptability facing different complex conditions.

4 Hierarchical Optimization

In this section, hierarchical optimization was adopted to improve the soft landing performance of the lander. The optimization took buffer parameters k, $c_{\max}$ and r as design variables, while the performance indexes U, L and S as three primary objectives. Since the change of the buffer parameters is followed with the change of the worst condition, the worst condition and corresponding performance indexes should be updated duly during the optimization process. Aiming at this complex optimization problem, a hierarchical optimization method was proposed decomposing the problem into a leader and several followers. After receiving the buffer parameters from the leader and modifying the model correspondingly, the followers took the conditioning factors as design variables to find the worst conditions respectively. Then the results of this "reverse optimizations" were delivered to the leader. The leader then optimized the buffer parameters trying to better the worst performance indexes. And the new buffer parameters determined by leader are transmitted to the followers to start the next iteration. The cycle continues until the terminating conditions are satisfied. Finally, the Pareto optimal set of the buffer parameters is obtained after hierarchical optimization.

But because this optimization method needs much more iterations, time cost will be much higher if the dynamic model is used to computed. Therefore, this paper uses the response surface model instead of time consuming dynamic analysis model to iterate, shortening the actual solution time and improve the optimization efficiency. In addition, the influence of the conditioning factors on the performance of soft landing is complex, so sensitivity analysis was carried out to determine the influence degree of each conditioning factor on the soft

Table 5 Parameters of 2-2 condition

Parameter	Value
v_x (m/s)	3.5
φ (°)	45
μ	0.7
α_e (°)	8

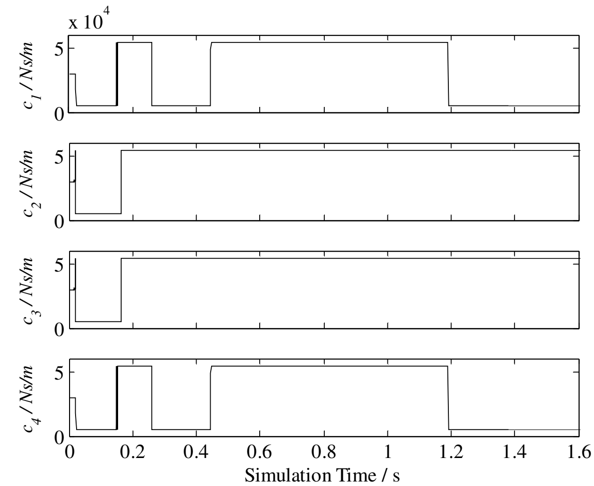

Figure 6 Damping coefficient of adaptive buffer

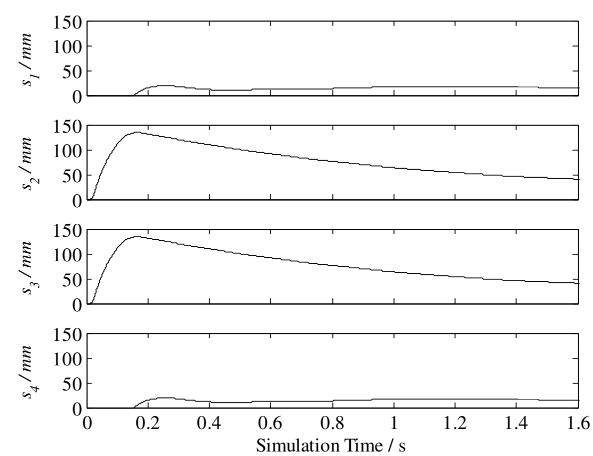

Figure 7 Buffer stroke of primary strut

landing performance before establishing response surfaces. To sum up, the flowchart of hierarchical optimization is shown in Figure 11.

4.1 Sensitivity Analysis of Conditioning Factors

The 36 results obtained from experimental design analyzing the landing performance in Section 3.2 is used as the sample points for sensitivity analysis. The Pareto diagram, which displays the sensitivity of 4 conditioning factors to landing indicators is shown in Figures 12, 13, 14 and 15. Here, the solid bars indicate positive effects while hollow bars mean negative effects. As the figures show, there are both positive and negative effects to 4 landing indicators, which means that four indicators are conflict with each other and one performance improvement often leads to the other performances lowered. In addition, the sensitivity analysis shows that the initial vertical velocity has

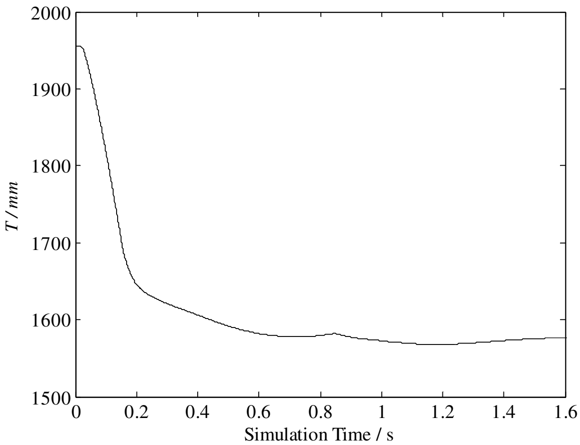

Figure 8 Landing stability index

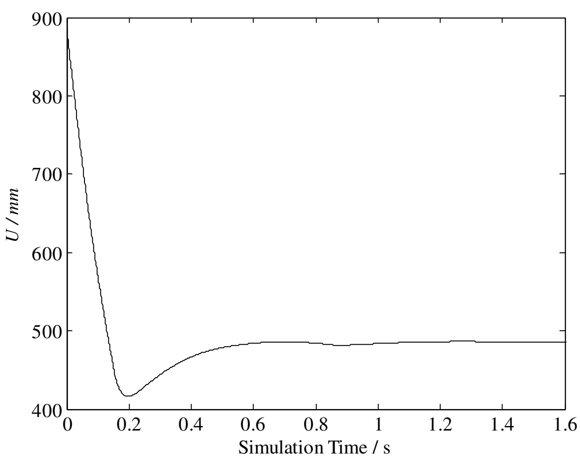

Figure 9 Nozzle's performance against damage

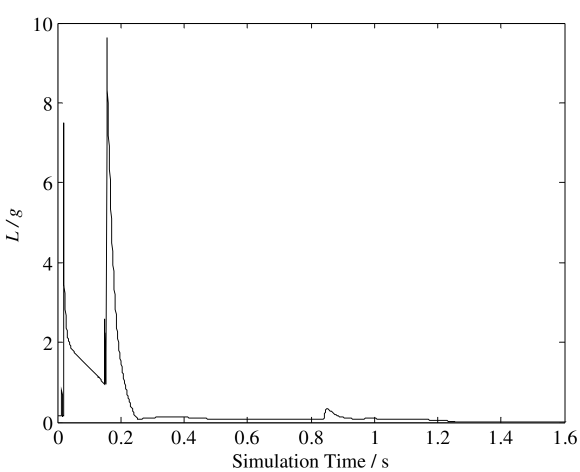

Figure 10 Acceleration overload

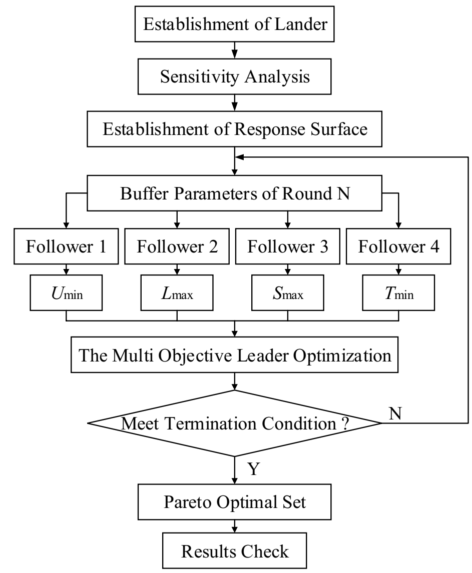

Figure 11 Flowchart of hierarchical optimization

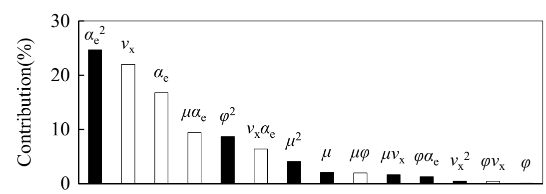

Figure 12 Sensitivity of conditioning factors to *U*

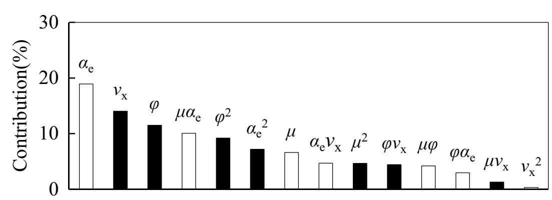

Figure 13 Sensitivity of conditioning factors to *L*

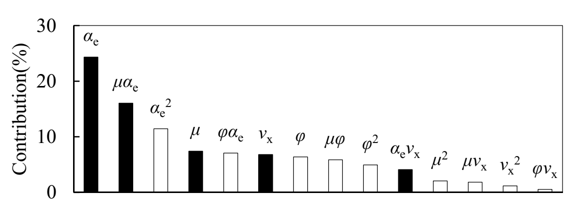

Figure 14 Sensitivity of conditioning factors to *S*

less influence on the stability distance. So v_x is neglected while establishing the response surface model of stability distance.

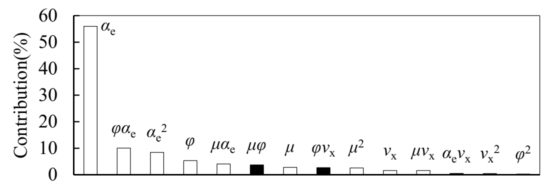

Figure 15 Sensitivity of conditioning factors to *T*

4.2 Response Surface Model

According to the results of sensitivity analysis, there was a complex coupling relation between the conditioning factors influencing the landing indicators. Thus, the incomplete three order polynomial function was selected to establish the response surface models, whose basic structure is shown as Eq. (3):

$$f(x) = \beta_0 + \sum_{i=1}^{n} \beta_i x_i + \sum_{ij(i<j)}^{n} \beta_{ij} x_i x_j + \sum_{i=1}^{n} \beta_{ij} x_i^2 + \sum_{i=1}^{n} \beta_{iii} x_i^3, \tag{3}$$

where x_i means input variables, n is the number of input variables and β is polynomial coefficients.

According to the process of the hierarchical optimization method, k, $c_{\max}$, r and v_x, ϕ, μ, α_e were chosen as input variables. 44 sample points were obtained by adopting the optimized Latin hypercube experimental design, which are listed as Table 11 in Appendix. The response surface model was established by least square fitting using the sample points, shown as Eqs. (7)–(10) in Appendix. The fitting precision of the response surface model was checked by two test methods, namely, root mean square error RMSE and the coefficient of multiple determination R^2. Their expressions are shown in Eqs. (4), (5) respectively:

$$\text{RMSE} = \frac{1}{m\bar{y}} \sqrt{\sum_{i=1}^{m} (y_i - \hat{y}_i)^2}, \tag{4}$$

$$R^2 = 1 - \frac{\sum_{i=1}^{m} (y_i - \hat{y}_i)^2}{\sum_{i=1}^{m} (y_i - \bar{y}_i)^2}, \tag{5}$$

where m is the number of sample points, y is the output value of sample point, $\hat{y}$ is the corresponding output value evaluated by responsible surface model, $\bar{y}$ is the mean of sample points. A little RMSE and a large R^2 mean a better model with high fitting precise.

Figure 16 shows the fitting degree by setting the landing indicators obtained from sample points as *X*-axis and the corresponding ones from response surface model under the same inputs as *Y*-axis. The closer the scatter points are to the middle diagonal line, the higher the fitting accuracy is.

In the figure, subscript *A* indicates that the values of landing indicators were obtained by simulation and subscript *P* means that they were from response surface model.

It can be seen from Figure 16 that the R^2 of all indicators are higher than 0.97, and RMSE less than 0.05. The fitting accuracy is enough for the response surface models to replace the dynamic one to be computed.

4.3 Optimization in the Followers

After being determined by the leader and transmitted to the followers, the buffer parameters remained unchanged in a round of sub optimization until the next iteration receiving the new parameters from the leader. The followers took landing conditioning factors as design variables, and the four worst landing indicators as objectives. The key parameters of the optimization mathematical models are listed in Table 6. Where q_i represent the buffer parameters v_x, ϕ, μ and α_e, while q_i^L, q_i^U are the lower and upper limits of the corresponding parameters respectively.

The evolution algorithm was adopted for the optimization calculation of the followers, and the algorithm parameters are listed in Table 7. Figure 17 shows iterative processes of four follower optimizations under initial buffer parameters (Table 2). Results show that optimization processes of four followers converged well, and the worst conditions could be found within the maximum iteration step.

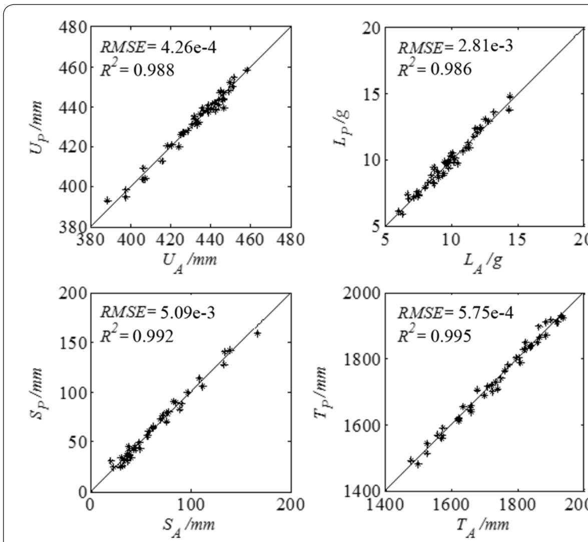

Figure 16 Scatter diagram for fitting precision of response surface

Table 6 Mathematical models of the follower optimizations

Number	Objective	Constraint	Output
1	Min U	$q_i^L < q_i < q_i^U$	U_{min}
2	Max L		L_{max}
3	Max S		S_{max}
4	Min T		T_{min}

Table 7 Configuration parameters of evolution algorithm

Parameter	Value
Max evaluation	200
Convergence tolerance	0.1
Minimum discrete step	0.02
Parallel batch size	5
Penalty base	0
Penalty multiplier	1000
Penalty exponent	2
Failed run penalty value	1×10^{30}
Failed run objective value	1×10^{30}

4.4 Optimization in the Leader

Considering the uncertainty of landing conditions, in the premise of ensuring the landing stability, the multi-objective optimization was carried out to minimize L_{max}, minimize S_{max} and maximize U_{min}; Taking k, c_{max} and r as design variables. Therefore, the mathematical model of the leader optimization is shown as Eq. (6). Where x_i represent the buffer parameters c_{max}, r and K, while x_i^L, x_i^U are the lower and upper limits of the corresponding parameters respectively. The second generation non inferiority sorting genetic algorithm (NSGA-II) is adopted for the leader optimization, and the parameters of algorithm are listed in Table 8.

$$\left.\begin{array}{ll} \min & L_{max}, S_{max}, -U_{min} \\ \text{s.t.,} & T_{min} > 1400, \\ & L_{max} < 15, \\ & x_i^L < x_i < x_i^U. \end{array}\right\} \tag{6}$$

After the hierarchical optimization, the Pareto optimal set of the multi-objective optimization problem is obtained (Table 12 of Appendix). Figure 18 shows the Pareto front fitted by the three performance indexes L_{max}, S_{max} and U_{min}. Considering the acceleration tolerance of precision equipment in the lander and human is sensitive to the change of acceleration, a small overload helps to improve the reliability of the lander. The optimum buffer parameters selected comprehensively from Pareto optimal set is shown in Table 9.

According to the selected optimum buffer parameters (Table 9), the dynamic analysis model was modified correspondingly. Then dynamic simulation was carried out again while using the 36 landing conditions the same as the experimental design in Section 3.2. Table 10 compares the calculation results before and

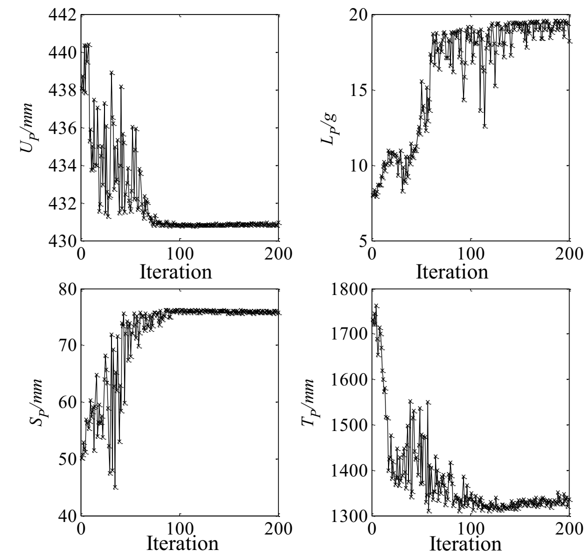

Figure 17 Iteration processes of four follower optimizations

Table 8 Configuration parameters of NSGA-II

Parameter	Value
Population size	12
Number of generation	20
Crossover probability	0.9
Crossover distribution index	10
Mutation distribution index	20

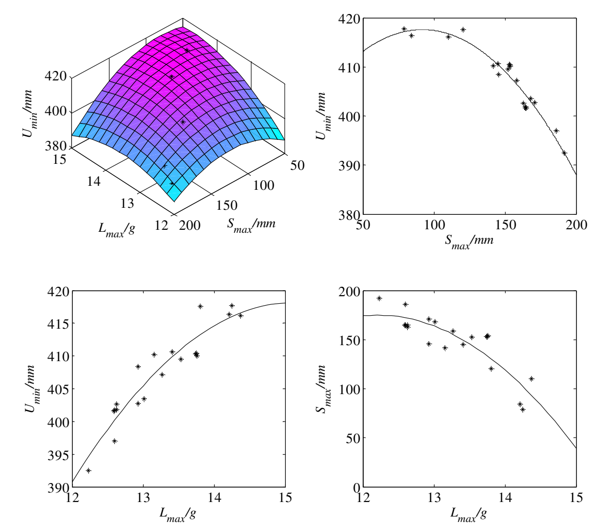

Figure 18 Pareto front of three performance indexes

Table 9 The selected buffer parameters

Parameter	c_{max} (Ns/m)	r	K (N/m)
Value	34224.47	0.30	50450.50

Table 10 Results of the hierarchical optimization

Landing performance index		U (mm)	L (g)	S (mm)
Before	Max.	432.9272	15.57734	186.1706
	Avg.	401.6185	9.827149	127.2947
	Min.	381.7005	5.600144	57.4495
After	Max.	439.0153	14.68367	146.8838
	Avg.	415.9362	9.536974	94.99342
	Min	401.6876	5.484198	38.52626

after optimization. The comparative analysis shows that the three landing performances have been improved to a certain extent under the premise of ensuring the stability of the lander not reduced. Under the respective worst conditions, nozzle performance against damage is increased by 5.24%, the acceleration overload is decreased by 5.74%, and the buffer performance of the primary strut is increased by 21.10%. As for the average, nozzle performance against damage is increased by 3.57%, the acceleration overload is decreased by 2.95%, and the buffer performance of the primary strut is increased by 25.38%.

5 Conclusions

1) The dynamic analysis model of the lander which is equipped with adaptive buffer was established. And the semi-active control algorithm is applied to realize the adaptive feedback adjustment of the damping coefficient during soft landing. Based on the dynamic analysis model and experimental design method, the soft landing performances under multiple landing conditions were analyzed.
2) Focusing on the worst landing condition uncertainty caused by the changes of buffer parameters, a hierarchical optimization method was proposed. The method divides the optimization problem into two parts, namely, a multi-objective leader optimization and several follower optimizations. Through this method, the worst condition was updated duly during optimization process. Furthermore, in order to improve the computational efficiency, response surface models were established to replace the dynamic models for iterative calculation.
3) The soft landing performances before and after the optimization were compared. In the premise of ensuring the landing stability not decline, nozzle's performance against damage, the buffer performance of the primary strut and the acceleration overload performance are all improved after optimizing. And the comparison results indicate the effectiveness of the hierarchical optimization method.
4) Those studies provide guidance to the design of adaptive lander, including the scheme determination, performance analysis and optimal design. And the hierarchical optimization method, which was proposed to solve complex optimization problems, provides a feasible scheme for optimal design of the project with similar properties.
5) The feasibility of the lander with adaptive buffer is validated preliminarily. However, the performances of the buffer such as vibration and response speed may also influence the soft landing performances in some way, which is simplified in this paper. In future studies, we intend to research on those properties respectively, thus validating its practicability further.

Authors' Contributions

CW was in charge of the whole trial; ZD wrote the manuscript; HW and JD assisted with sampling and laboratory analyses. All authors read and approved the final manuscript.

Author Details

[1] School of Mechanical Engineering and Automation, Beijing University of Aeronautics and Astronautics, Beijing 100083, China. [2] Beijing System Design Institute of Electro-Mechanic Engineering, China Aerospace Science and Industry Corporation Limited, Beijing 100854, China. [3] Department of Mechanical Engineering, Tsinghua University, Beijing 100084, China. [4] State Key Laboratory of Virtual Reality and Systems, Beijing University of Aeronautics and Astronautics, Beijing 100083, China.

Authors' Information

Zongmao Ding, born in 1993, is currently a master candidate at *School of Mechanical Engineering and Automation, Beijing University of Aeronautics and Astronautics, China*. He received his bachelor degree from *Beijing University of Aeronautics and Astronautics, China*, in 2016.

Hongyu Wu, born in 1993, is currently a PhD candidate at *Department of Mechanical Engineering, Tsinghua university, China*. He received his master degree from *Beijing University of Aeronautics and Astronautics, China*, in 2018.

Chunjie Wang, born in 1955, is currently a professor at *State Key Laboratory of Virtual Reality and Systems, Beijing University of Aeronautics and Astronautics, China*. She received her PhD degree from *China University of Mining and Technology, China*, in 1997.

Jianzhong Ding, born in 1991, is currently a PhD candidate at *School of Mechanical Engineering and Automation, Beijing University of Aeronautics and Astronautics, China*. He received his bachelor degree from *China University Of Petroleum, China*, in 2013.

Competing Interests

The authors declare that they have no competing interests.

Funding

Supported by National Natural Science Foundation of China (Grant No. 51635002).

Appendix

See Tables 11 and 12.

Table 11 Sample points for response surface

Number	Landing conditioning factor				Buffer parameter			Soft landing indicator			
	v_x (m/s)	φ (°)	μ	α_e (°)	k (N/m)	c_{max} (Ns/m)	r	U (mm)	L (g)	S (mm)	T (mm)
1	3.55814	25.11628	0.625581	9.069767	38372.09	35581.4	0.916279	443.7838	7.475721	72.63525	1525.675
2	3.093023	7.325581	0.616279	6.27907	43023.26	57906.98	0.895349	451.6653	7.177718	39.61241	1699.808
3	3.186047	43.95349	0.45814	4.418605	55116.28	64418.6	0.225581	431.4194	10.88976	62.80241	1750.597
4	3.651163	37.67442	0.318605	1.860465	36511.63	60697.67	0.560465	436.2251	12.84088	36.68639	1867.666
5	3.860465	23.02326	0.430233	7.674419	49534.88	66279.07	0.12093	397.3568	9.527114	134.2162	1622.154
6	3.511628	18.83721	0.644186	2.093023	41162.79	68139.53	0.372093	435.8223	11.07385	48.61199	1860.488
7	3.465116	40.81395	0.672093	6.511628	59767.44	56976.74	0.874419	458.2829	6.729019	35.81923	1575.491
8	3.069767	6.27907	0.532558	5.813953	50465.12	52325.58	0.1	406.1348	6.315581	138.9933	1741.022
9	3.767442	20.93023	0.569767	1.627907	34651.16	50465.12	0.97907	439.0863	12.59231	30.0238	1864.758
10	3.023256	21.97674	0.439535	0.232558	37441.86	47674.42	0.434884	446.5893	12.19919	30.33212	1937.609
11	3.744186	45	0.411628	4.883721	45813.95	30930.23	0.665116	428.6257	10.1308	58.0304	1720.903
12	3.27907	23.02326	0.402326	3.488372	60697.67	30000	0.204651	406.2816	8.617354	108.5894	1802.934
13	3.953488	11.51163	0.662791	7.906977	50465.12	59767.44	0.686047	438.8208	8.01536	69.29281	1557.978
14	3.906977	19.88372	0.57907	8.604651	43953.49	31860.47	0.246512	388.0991	7.463903	167.2496	1570.922
15	4.000000	33.48837	0.486047	2.790698	63488.37	61627.91	0.623256	433.1043	13.22439	39.97564	1820.304
16	3.395349	15.69767	0.327907	5.581395	33720.93	39302.33	0.853488	438.4899	9.852899	42.87013	1722.803
17	3.232558	34.53488	0.7	4.651163	42093.02	37441.86	0.309302	420.6606	8.718477	90.62936	1734.21
18	3.348837	38.72093	0.3	4.186047	67209.3	49534.88	0.727907	442.5974	10.22104	33.63026	1760.997
19	3.139535	41.86047	0.54186	5.116279	30000	56046.51	0.769767	450.9664	8.521337	33.12291	1710.982
20	3.627907	39.76744	0.523256	8.139535	68139.53	43953.49	0.288372	424.03	9.826323	85.53164	1571.029
21	3.116279	17.7907	0.346512	6.744186	39302.33	70000	0.497674	446.3383	9.665368	38.22251	1678.262
22	3.511628	2.093023	0.504651	9.534884	30930.23	53255.81	0.455814	434.7544	8.284954	75.42411	1623.473
23	3.604651	8.372093	0.309302	8.837209	56976.74	42093.02	0.393023	424.9629	9.848023	70.92657	1623.236
24	3.000000	31.39535	0.448837	9.302326	52325.58	41162.79	0.602326	446.6824	7.551606	56.10278	1527.46
25	3.813953	14.65116	0.355814	0.465116	56046.51	36511.63	0.706977	431.8234	14.37905	37.44909	1931.803
26	3.697674	16.74419	0.467442	6.976744	66279.07	40232.56	1	439.2425	9.958682	44.41087	1660.581
27	3.209302	26.16279	0.634884	1.162791	69069.77	50465.12	0.413953	441.5735	11.85765	36.75207	1903.21
28	3.581395	0	0.597674	0.697674	61627.91	55116.28	0.811628	444.0431	14.35065	22.20284	1920.56
29	3.325581	10.46512	0.681395	8.372093	64418.6	38372.09	0.539535	433.6575	6.023513	97.01569	1568.123
30	3.418605	31.39535	0.393023	6.976744	31860.47	43023.26	0.162791	397.4444	8.962404	133.354	1635.542
31	3.976744	9.418605	0.42093	3.023256	32790.7	48604.65	0.330233	415.4679	11.31945	82.85015	1841.057
32	3.488372	12.55814	0.337209	0.930233	57906.98	62558.14	0.267442	432.064	12.23215	49.46587	1918.122
33	3.046512	3.139535	0.374419	3.72093	62558.14	45813.95	0.727907	444.9144	8.697139	37.0097	1824.333
34	3.674419	35.5814	0.383721	9.767442	46744.19	57906.98	0.790698	449.4951	10.30864	38.29463	1501.226
35	3.302326	29.30233	0.653488	10	44883.72	63488.37	0.351163	446.2622	6.831806	89.31796	1478.876
36	3.44186	1.046512	0.57907	3.255814	40232.56	32790.7	0.518605	426.7935	8.704603	75.62599	1825.387
37	3.837209	5.232558	0.560465	3.953488	65348.84	46744.19	0.183721	407.39	9.410543	111.8682	1795.231
38	3.790698	4.186047	0.365116	5.116279	48604.65	65348.84	0.832558	441.3873	11.94245	31.54661	1772.535
39	3.930233	42.90698	0.606977	6.046512	35581.4	54186.05	0.476744	430.4629	10.50151	62.02561	1659.939
40	3.883721	27.2093	0.690698	2.55814	57906.98	34651.16	0.644186	426.3876	11.67777	57.27592	1810.075
41	3.372093	13.60465	0.495349	7.44186	70000	67209.3	0.560465	444.9501	9.049236	44.0253	1656.702
42	3.162791	30.34884	0.551163	2.325581	53255.81	33720.93	0.95814	441.7665	9.359383	38.15687	1838.727
43	3.697674	36.62791	0.504651	0	47674.42	44883.72	0.14186	418.4696	14.45879	78.39083	1885.561
44	3.255814	28.25581	0.476744	1.395349	54186.05	69069.77	0.937209	449.1199	11.39628	19.53422	1886.16

Table 12 Pareto optimal set

Number	Buffer parameter			Soft landing indicator			
	k (N/m)	c_{max} (Ns/m)	*r*	*U* (mm)	*L* (*g*)	*S* (mm)	*T* (mm)
1	48645.04	32631.58	0.54	410.35	13.74	153.41	1377.71
2	52918.01	34182.02	0.38	403.50	13.01	168.24	1378.14
3	48847.99	42448.80	0.32	402.64	12.63	162.80	1382.14
4	37868.15	43615.22	0.46	410.62	13.41	145.24	1424.04
5	48645.04	32631.58	0.54	410.46	13.75	153.15	1382.12
6	52939.73	34181.47	0.49	409.54	13.53	152.26	1373.57
7	50450.50	34224.47	0.30	397.01	12.60	186.01	1381.92
8	47405.10	43285.34	0.57	416.40	14.21	84.27	1374.32
9	54412.82	42293.62	0.56	416.17	14.37	110.07	1364.38
10	49043.65	34030.66	0.38	402.70	12.93	170.88	1384.36
11	51254.63	34224.47	0.45	407.17	13.27	158.45	1378.37
12	47405.10	46200.59	0.57	417.59	13.81	120.30	1378.44
13	51741.07	41959.17	0.21	392.47	12.23	191.89	1372.44
14	51747.93	41959.17	0.43	410.24	13.15	141.71	1382.74
15	51741.07	42750.60	0.30	401.69	12.60	165.04	1376.91
16	47464.88	45073.37	0.38	408.42	12.93	145.43	1383.79
17	52631.88	42750.60	0.30	401.87	12.63	164.55	1375.59
18	50468.09	42106.01	0.30	401.58	12.59	164.61	1399.94
19	53901.44	32375.72	0.52	410.03	13.76	153.74	1371.07
20	48096.98	46328.25	0.57	417.70	14.25	79.17	1372.52

$$\begin{aligned} U =\,& 511.59 - 1.1048\varphi - 199.74\mu + 205.45r \\ & - 6.9518\alpha_e - 24.145v_x + 0.015802\varphi^2 + 68.985\mu^2 \\ & - 253.31r^2 + 0.43316\alpha_e^2 + 0.76387\varphi\mu + 2.3551\text{E} \\ & - 6\varphi k + 7.8933\text{E} - 4\mu c_{\max} + 2.3759\text{E} - 4\mu k \\ & + 19.753\mu v_x - 2.2695\text{E} - 6c_{\min} + 3.9774\alpha_e c_{\max} \\ & + 3.8669r\alpha_e - 3.2941\text{E} - 4rk + 2.1381\alpha_e k \\ & - 0.76569\alpha_e v_x + 121.85r^3, \end{aligned} \tag{7}$$

$$\begin{aligned} L =\,& 26.775 - 5.0093r - 0.48742\alpha_e + 14.621\mu^2 \\ & + 0.11214\alpha_e^2 - 6.7505\text{E} - 9k^2 - 3.4301v_x^2 \\ & + 0.071897\varphi\mu - 0.13375\varphi r - 8.0912\text{E} \\ & - 5\mu c_{\max} - 1.4029\mu\alpha_e - 2.9661\mu v_x \\ & - 2.8717\text{E} - 5c_{\max}r - 1.8059\text{E} - 6\alpha_e c_{\max} \\ & + 2.5342rv_x - 0.10076\alpha_e v_x + 5.0199\text{E} - 5kv_x \\ & + 3.1638\text{E} - 5\varphi^3 + 1.1452\text{E} - 14c_{\max}^3 \\ & + 1.1324r^3 + 6.5243\text{E} - 14k^3 + 0.67529v_x^3, \end{aligned} \tag{8}$$

$$\begin{aligned} S =\,& 482.67 - 0.0052582c_{\max} - 615.95r + 193.76\mu^2 \\ & + 4.2096\text{E} - 8c_{\max}^2 + 777.24r^2 - 33.976v_x^2 \\ & - 1.7764\varphi\mu + 1.0444\text{E} - 5\varphi c_{\max} \\ & + 0.41149\varphi r + 9.5027\mu\alpha_e - 44.733\mu v_x \\ & + 4.9696\text{E} - 4c_{\max}r - 6.6522\text{E} - 5c_{\max}\alpha_e \\ & - 5.0897r\alpha_e + 5.7483\text{E} - 4rk + 1.6141\alpha_e v_x \\ & + 3.8669r\alpha_e - 5.0606\text{E} - 4kv_x - 7.8106\text{E} \\ & - 5\varphi^3 - 357.00r^3 + 1.5838\text{E} - 13k^3 + 7.9416v_x^3, \end{aligned} \tag{9}$$

$$\begin{aligned} T =\,& 15524 - 0.35713\varphi + 1102.9\mu + 239.20r \\ & - 11976v_x + 8.9406\text{E} - 9c_{\max}^2 - 593.63r^2 \\ & - 3.3219\alpha_e^3 + 3437.5v_x^2 - 0.22014\varphi\alpha_e \\ & - 0.0014584\mu c_{\max} - 11.325\mu\alpha_e - 0.0027737\mu k \\ & - 218.04\mu v_x - 6.3259r\alpha_e + 29.639rv_x - 1.9831\text{E} \\ & - 4\alpha_e k - 213.08\mu^3 + 315.93r^3 + 0.15724\alpha_e^3 \\ & + 2.9960\text{E} - 13k^3 - 325.27v_x^3. \end{aligned} \tag{10}$$

Received: 14 June 2017 Accepted: 18 February 2019
Published online: 12 March 2019

References

[1] Schröder S, Reinhardt B, Brauner C, et al. Development of a Marslander with crushable shock absorber by virtual and experimental testing. *Acta Astronautica*, 2017, 134: 65–74.
[2] Y Zhang, H Nie, J B Chen. Design and analysis of MR bumper about lunar damper soft landing. *Aerospace Shanghai*, 2009, 26(1): 48–52. (in Chinese)
[3] G H Lucas, H D Robert, J M Veloria. *Modeling and validation of a navy A6-intruder actively controlled landing gear system*. NASA Langley Technical Report Server, 1999.
[4] J Holnickiszulc, P Pawłowski, M Mikułowski, et al. Adaptive impact absorption and applications to landing devices. *Advances in Science & Technology*, 2008, 56: 609–613.
[5] M Ostrowski, J Holnicki-Szulc. Adaptive impact absorption controlled via pyrotechnic devices. *4th European Conf. on Structural Control*, Petersburg, Russia, 2008.
[6] J H Hu. *Research on magnetorheological fluid damping semi-active control system*. Zhejiang University, 2007. (in Chinese)
[7] Q Zhou. *Design and analysis of magneto rheological dynamic vibration absorber*. Huazhong University of Science and Technology, 2013. (in Chinese)
[8] L Sa. *Design of magnetorheological buffer for lunar lander soft landing gear*. Beijing Jiaotong University, 2016. (in Chinese)
[9] B Y Niu. *Structure design and optimization of magnetorheological buffer for lunar lander landing system*. Chongqing University, 2016. (in Chinese)
[10] G M Mikulowski, J Holnickiszulc. Adaptive landing gear concept—feedback control validation. *Smart Materials & Structures*, 2007, 16(6): 2146.
[11] A L Wang. *Research on dynamics and semi-active control of lunar lander soft landing*. Nanjing University of Aeronautics & Astronautics, 2011. (in Chinese)
[12] G Mikulowski, L Jankowski. Adaptive landing gear: Optimum control strategy and potential for improvement. *Shock & Vibration*, 2015, 16(2): 175–194.
[13] T Maeda, M Otsuki, T Hashimoto, et al. Attitude stabilization for lunar and planetary lander with variable damper. *Journal of Guidance, Control, and Dynamics*, 2016: 1790–1804.
[14] J J Wang, C J Wang, S G Song. Performance optimization of lunar lander based on response surface methodology. *Journal of Beijing University of Aeronautics and Astronautics*, 2014, 40(5): 707–711. (in Chinese)
[15] H Y Wu, C J Wang, J Z Ding, et al. Soft landing performance optimization for novel lander based on multiple working conditions. *Journal of Beijing University of Aeronautics and Astronautics*, 2017(4): 776–781. (in Chinese)
[16] Q X Qin, X Qin, J R Xiao, et al. Robust optimization design of the mars airbag lander. *China Mechanical Engineering*, 2017, 28(1): 20–26. (in Chinese)
[17] J Z Yang, F M Zeng, J F Man, et al. Design and verification of the landing impact attenuation system for Chang'E-3 lander. *Scientia Sinica (Technologica)*, 2014(5): 440–449. (in Chinese)
[18] H Y Chai, Y H Deng, C Sheng. Design and realization of structure subsystem for the Chang'E-3 lunar lander. *Scientia Sinica (Technologica)*, 2014(4): 391–397. (in Chinese)
[19] X X Bai, N M Wereley, W Hu. Maximizing semi-active vibration isolation utilizing a magnetorheological damper with an inner bypass configuration. *Journal of Applied Physics*, 2015, 117(17): 288.
[20] X X Bai, W Hu, N M Wereley. Magnetorheological damper utilizing an inner bypass for ground vehicle suspensions. *IEEE Transactions on Magnetics*, 2013, 49(7): 3422–3425.
[21] A L Wang, H Nie, J B Chen. State-jump semi-active control of lunar lander soft landing. *Acta Aeronautica Et Astronautica Sinica*, 2009, 30(11): 2218–2223. (in Chinese)
[22] Z W Li, Z J Li. Status of researching on dynamical models of MR damper. *Machine Building & Automation*, 2012, 41(1): 142–145. (in Chinese)
[23] Y H Guo, E W Chen, Y M Lu, et al. Calculation of equivalent linear damping coefficient of a magnetorheological damper. *China Mechanical Engineering*, 2014, 25(13): 1719–1723. (in Chinese)
[24] Z Q Deng, S C Wang, H B Gao, et al. Upper limit amplitude of lunar lander based on ADAMS software. *Journal of Harbin Institute of Technology*, 2003, 35(12): 1492–1495. (in Chinese)
[25] "LORD Technical Data RD-8040-1 and RD-8041-1 Dampers," Accessed on November 2015, www.lordfulfillment.com/upload/DS7016.pdf.
[26] R J Muraca, J W Campbell, C A King. *A Monte Carlo analysis of the viking lander dynamics at touchdown*. National Aeronautics and Space Administration, 1975.
[27] R E Lavender. *Monte Carlo approach to touchdown dynamics for soft lunar landings*. NASA-TN-D-3117, 1965.